Dicarbon antisite defect in n-type 4H-SiC

doi: 10.1103/PhysRevB.79.115211

Dicarbon antisite defect in *n*-type 4*H*-SiC

T. Umeda and J. Isoya
Graduate School of Library, Information and Media Studies, University of Tsukuba, Tsukuba 305-8550, Japan

N. Morishita and T. Ohshima
Japan Atomic Energy Agency, Takasaki 370-1292, Japan

E. Janzén
Department of Physics, Chemistry, and Biology, Linköping University, SE-581 83 Linköping, Sweden

A. Gali
Department of Atomic Physics, Budapest University of Technology and Economics, Budafoki út 8., H-1111 Budapest, Hungary

(Received 13 August 2008; revised manuscript received 5 January 2009; published 24 March 2009)

We identify the negatively charged dicarbon antisite defect (C_2 core at silicon site) in electron-irradiated *n*-type 4*H*-SiC by means of combined electron paramagnetic resonance (EPR) measurements and *first-principles* calculations. The HEI5 and HEI6 EPR centers ($S=1/2$; C_{1h} symmetry) are associated with cubic and hexagonal dicarbon antisite defects, respectively. This assignment is based on a comparison of the measured and calculated hyperfine tensors of ^{13}C and ^{29}Si atoms as far as the second neighborhood around the defects. Theoretically, the dicarbon antisites are stable in a single negative charge state under a wide range of *n*-type samples. We found that the defects can be created under a wide range of irradiation conditions, and our measurements strongly suggest the existence of carbon antisite defects in the *as-grown* samples. Annealing studies revealed several atomistic processes such as recombination of carbon interstitials with vacancies and formation of carbon aggregates. These processes were activated at about 1000 °C, and as theoretically predicted, the dicarbon antisite is much more stable than the dicarbon interstitial defect (C_2 core at carbon site). The measured activation temperature is consistent with the temperature range for forming various carbon aggregate-related photoluminescence centers.

DOI: 10.1103/PhysRevB.79.115211 PACS number(s): 61.72.J−, 71.55.Ht, 71.15.Mb, 76.30.Mi

I. INTRODUCTION

Silicon carbide (SiC) is unlike other wide-band-gap semiconductors (GaN, ZnO, diamond, etc.) because large-diameter pure single crystals can be grown. Furthermore, SiC potentially has uses in power electronic devices of high performance. A problem is that SiC technology has not progressed far enough to be able to control defects that may affect SiC crystals; even the basic defects are not entirely understood. In recent years, though, significant progress has been made in identifying vacancy defects.[1] Their identification has mostly been through a combination of electron paramagnetic resonance (EPR) spectroscopy and first-principles calculations. In fact, we can now list many examples of vacancy defects in 4*H*-SiC: V_{Si}^- (V_{Si}^- and T_{V2a}),[2] V_C^+ (EI5/6),[3] V_C^- (HEI1),[4] $C_{Si}V_C^+$ (HEI9/10),[5] $C_{Si}V_C^-$ (SI5),[6] and $V_{Si}V_C^0$ (*P*6/7).[7] Some of these defects have also been identified in 6*H*-SiC and other polytypes.[1] These vacancy defects can be generated by electron, neutron, and ion irradiation and subsequent annealing. They also appear in as-grown crystals.[8]

In principle, the formation of vacancies must be accompanied by the formation of silicon or carbon interstitials (Si_i and C_i). In fact, theoretical studies predict a number of possible interstitial-related defects in SiC.[9–13] Carbon interstitials are especially important because they are highly mobile[9,11] and are able to form very stable aggregates owing to strong C-C bonds.[9–13] The C_i atom can be energetically stabilized by a dumbbell or dicarbon structure (C_2) at either the C site or Si site. The former is a dicarbon interstitial defect (or carbon split interstitial) $(C_2)_C$, which is mobile, and it aggregates relatively easy with other interstitials forming clusters[9,10] The latter type is called dicarbon antisite $(C_2)_{Si}$,[9,10] which is produced by pairing C_i and a carbon antisite (C_{Si}), and it exhibits higher thermal stability.[9,10,12] At high temperatures, these dicarbon defects can produce a variety of carbon-interstitial-related defects such as $[(C_2)_C]_2$,[9,11] $[(C_2)_{Si}]_2$,[9,10] $(C_2)_{Si}$-$(C_2)_C$,[9] and $(C_3)_{Si}$.[9,10,13] They are therefore possible stable defects that are generated by high temperature annealing. For example, some of them are considered to be the origin of the D_{II} center [a group of $(C_2)_{Si}$],[9,10] *P*-*T* centers [$(C_2)_C$],[9] and *U*, *Z*, HT3, HT4, and HT5 centers [$(C_3)_{Si}$ and their family][13] in photoluminescence (PL) spectroscopy or to the $Z_{1/2}$ centers [a ring structure made of $(C_2)_{Si}$ and C_i][12] in deep-level transient spectroscopy (DLTS). Moreover, Steeds *et al.*[14] recently presented the most successful assignment so far from PL measurements. For 4*H*-SiC, they assigned a set of four 463 nm luminescence lines to the four neutral states of $(C_2)_{Si}$.[14] Furthermore, they found that many other PL centers were possibly related to carbon-interstitial-related defects.[15] Their common signature is high-energy local vibration modes ($\geq$100 meV),[15] which can be generated by strong C-C bonds.[9–13]

Unfortunately, the PL measurements on the carbon-interstitial-related defects were successful in heavy irradiation conditions (10^{19}–10^{20} e/cm^2). Moreover, PL signals do not indicate the absolute concentrations of defects because their intensity is dependent on a complicated competition between excitation and emission processes. For example, the

463 nm (2.67 eV) signal mentioned above involves an up-conversion mechanism (emitted photon energy > excitation photon energy) owing to a coupling of other unknown centers.[14] Because of this, the formation and annihilation behaviors that can be seen in the 463 nm signal do not simply reflect those of $(C_2)_{Si}$.

Likewise, other spectroscopic techniques have only been partially successful in identifying carbon-interstitial-related defects. So far, EPR and theoretical studies have suggested dicarbon interstitial defects $(C_2)_C$ in as-irradiated SiC. For instance, the EI1/3 EPR centers (electron spin $S=1/2$ or 1; C_{1h} symmetry)[16] that were observed in room-temperature irradiated *p*-type 4*H*-SiC ($\geq 1\times 10^{17}$ e/cm^2) are theoretically due to positive or neutral charge states of $(C_2)_C$.[9] Subsequently, in room-temperature irradiated *n*-type 6*H*-SiC ($>1\times 10^{18}$ e/cm^2), a similar EPR center (the EI*n* center, $S=1$; C_{1h} symmetry) was observed under photoexcitation, and it was assigned to $(C_2)_C$ in the double positively charged state.[17] These centers were annihilated with a 200–300 °C anneal,[16,17] and this result reflects the low thermal stability of $(C_2)_C$ defects. However, the spectroscopic information on these centers is far from enough for making a conclusive identification. In particular, hyperfine (HF) interactions of interstitial carbon atoms, which are the most crucial information for identification, are not exactly known. Such HF interactions have yet to be detected for EI1/3, and have been investigated only at a single angle for EI*n*.[16,17]

In this paper, we present EPR and first-principles theoretical studies on an important carbon-interstitial defect, dicarbon antisite $(C_2)_{Si}$, in 4*H*-SiC. We found that electron irradiation very easily generated $(C_2)_{Si}$ defects in *n*-type 4*H*-SiC. We labeled the EPR signals of $(C_2)_{Si}$ as HEI5/6 ($S=1/2$; C_{1h} symmetry). By optimizing experimental conditions, their weak HF interactions due to a ^{13}C atom (nuclear spin $I=1/2$; natural abundance=1.1%) at an interstitial site were successfully revealed without isotope enrichments. In addition, HF interactions due to surrounding ^{29}Si atoms ($I=1/2$; natural abundance=4.7%) atoms were also analyzed. Comparing between the experimental results and theoretical calculations, the HEI5/6 centers were assigned to negative charge states of $(C_2)_{Si}$ at either cubic (k) or hexagonal (h) sites of 4*H*-SiC. Furthermore, we used EPR to reveal the formation and annihilation behaviors of $(C_2)_{Si}$.

II. EPR ANALYSIS

The EPR measurements were carried out with a Bruker BioSpin X-band cw-EPR spectrometer equipped with an Oxford ESR900 cryostat system. The spectra were measured using magnetic-field modulation at 100 kHz and a 0.05 mT width. Most of the measurement temperatures were chosen to be between 200 and 295 K since the detection of the HEI5/6 signals at low temperature is affected by a microwave saturation effect. All EPR data shown in this section were obtained at thermal equilibrium (without photoillumination).

The 1.5-mm-thick 4*H*-SiC samples were prepared using commercial nitrogen-doped substrates (room-temperature carrier concentration=$10^{17}/cm^3$). We prepared two types of sample with different crystal orientations; they exhibited different angular maps of the defect with respect to magnetic-field (**B**) rotations and thus were quite useful for angular-map analyses. The samples were subjected to 3 MeV electron irradiation at different temperatures (T_{irr}) inside a vacuum chamber of a radiation facility at the Japan Atomic Energy Agency. As demonstrated in our previous study,[5] a combination of our special thick samples and a high-*Q*-factor microwave cavity (over 10 000 factor under actual measurements) enabled us to resolve weak ^{13}C HF structures without isotope enrichments.

We already reported the HEI5/6 centers as "unknown defects" in Refs. 6 and 18. A typical EPR spectrum of these centers is shown in Fig. 1(a). They were the dominant paramagnetic defects in the thermal equilibrium state of irradiated *n*-type 4*H*-SiC. We found that the two signals had different microwave saturation behaviors. The HEI5 signal was

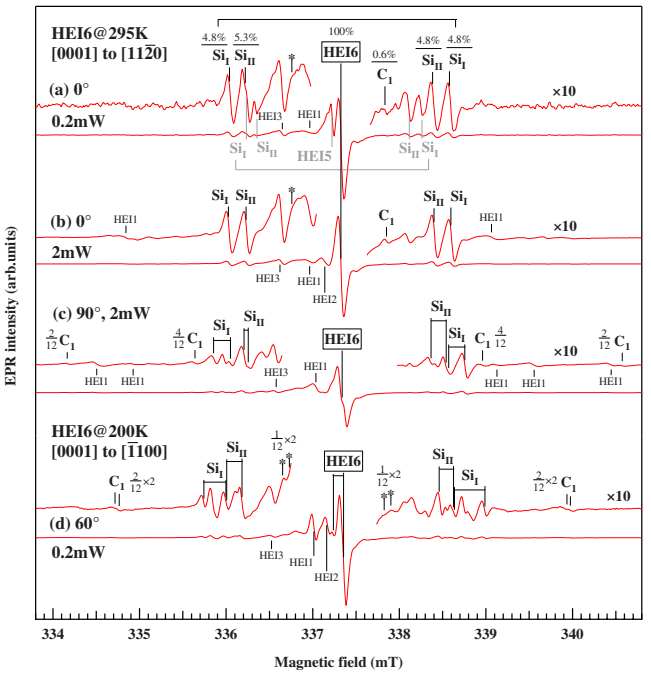

FIG. 1. (Color online) Hyperfine structures of HEI6 center in 4*H*-SiC. (a) and (b) 0° spectra of HEI6 measured during magnetic-field rotation from [0001] (0°) to [11$\bar{2}$0] (90°) with microwave of 0.2 and 2 mW (9.452 GHz), respectively. In (b), HEI5 signal was effectively suppressed due to a strong microwave saturation effect. Both spectra (a) and (b) showed four ^{29}Si HF satellite lines (Si_I and Si_{II}) and a high-field-side ^{13}C HF satellite line (C_1) of HEI6. In (a), we estimated intensity ratio of each satellite line to a central line for HEI6. Asterisks (*) indicate positions of missing ^{13}C satellite lines that are hidden by other strong signals. (c) 90° spectrum of HEI6. With this direction, C_1 HF structure splits into four satellite lines with intensity ratio of 2:4:4:2 [see an angular map in Fig. 4(a)], which were successfully resolved in this spectrum. (d) 60° spectrum of HEI6 measured during magnetic-field rotation from [0001] to [$\bar{1}$100] using microwave of 0.2 mW (9.428 GHz) at 200 K. For this spectrum, magnetic-field values are shifted to adjust to the case of 9.452 GHz. In this rotation experiment, C_1 HF structure splits into eight lines with a ratio of 2:2:1:1:1:1:2:2 [see an angular map in Fig. 4(c)], and outer four lines can be seen.

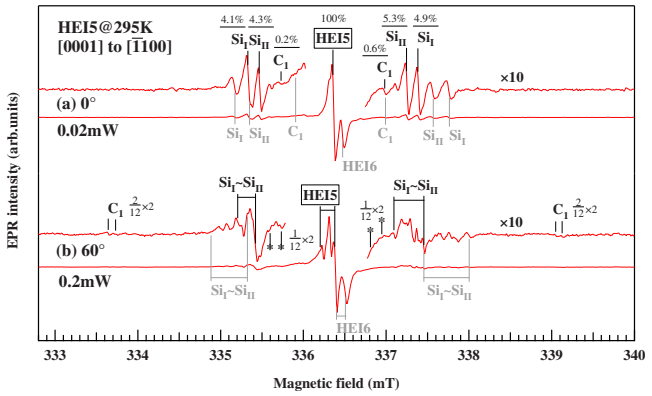

FIG. 2. (Color online) Hyperfine structures of HEI5 center in 4*H*-SiC. (a) 0° spectrum of HEI5 measured during magnetic-field rotation from [0001] (0°) to [$\bar{1}$100] (90°) using microwave of 0.02 mW (9.428 GHz). In this condition, both HEI5 and HEI6 signals were detected at the same time without microwave saturation behavior. We give intensity ratio of each HF satellite line to a central line for HEI5, supposing that overlapped HEI6's HF lines have their ideal intensities (9.4% for Si_I and 0.55% for C_1). (b) 60° spectrum of HEI5. C_1 HF structure of HEI5 splits into eight satellite lines with intensity ratio of 2:2:1:1:1:1:2:2 [see an angular map in Fig. 4(b)], and outer four lines can be resolved. Asterisks (*) indicate positions of missing ^{13}C satellite lines of HEI5.

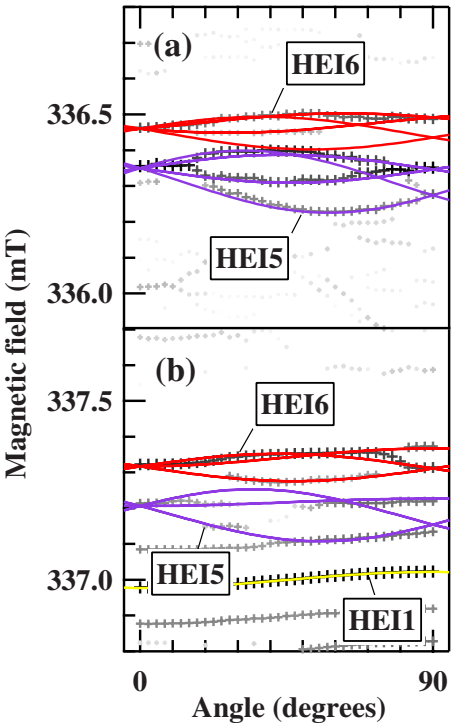

FIG. 3. (Color online) Angular maps of HEI5/6 centers (primary lines). The magnetic field was rotated by 90° in the following directions: (a) [$\bar{1}$100] and (b) [0001]→[11$\bar{2}$0]. Solid lines show simulated angular patterns. EPR measurements were carried out under the same conditions as in the measurements of Fig. 1(a). These maps were measured using different microwave frequencies.

rather easily saturated with a high microwave power. Therefore, using strong microwaves, we could selectively observe the HEI6 signal, as is shown in Figs. 1(b)–1(d). For the best symmetrical direction [0° or **B**∥[0001], Figs. 1(a) and 1(b)], two strong HF doublet structures (four HF satellite lines) and one weak HF doublet one (a low-field-side line was hidden by the HEI1 and HEI3 signals) can be resolved for HEI6. We call the strong outer and inner doublets "Si_I" and "Si_{II}", respectively, because they originate from ^{29}Si HF interactions. The relative intensities of each doublet to the central line were estimated to be, respectively, 9.6% and 10.1% for the Si_I and Si_{II} doublets [Fig. 1(a); in this spectrum, the HEI6 center exhibited almost no microwave saturation]. In the other spectrum, the intensity ratios were found to be 8.9% and 9.2%, respectively. These ratios are close to twice the ^{29}Si concentration (9.34%). Therefore, the wave function of HEI6 should extend over at least four Si atoms (two Si_I atoms and two Si_{II} atoms). The weak doublet is named "C_1", and it originates from a ^{13}C HF interaction. The high-field-side C_1 line shows a relative intensity of 0.6% to the central line in Fig. 1(a). This value varied between 0.3 and 0.8% among different spectra. Finally, we judged that the intensity ratio of the high-field-side C_1 line matches half the concentration of ^{13}C (1.11%÷2=0.55%). Namely, the HEI6 center should include one carbon atom in its core. This conclusion is quite reasonable because later analyses will show that more than 50% of the wave function of HEI6 is localized on this carbon atom. Therefore, no one can assume two or more carbon atoms for the C_1 HF structure.

The case of the HEI5 center is shown in Fig. 2. To observe HEI5, we must use a lower microwave power (e.g., <0.5 mW at 295 K). In Fig. 2, both HEI5/6 signals were observed at the same time. The features of HEI5 were very similar to those of HEI6. In Fig. 2(a) [0° or **B**∥(0001)], we found again the Si_I and Si_{II} HF doublets as well as the C_1 doublet for HEI5. The intensity ratios are also similar to those of HEI6: 9.0% and 9.6% for the Si_I and Si_{II} doublets, respectively, and 0.8% for the C_1 doublet in Fig. 2(a). Namely, both the HEI5/6 centers have the same atomic structure that consists of one carbon atom and four Si atoms. These atoms correspond to a central carbon interstitial atom and surrounding Si atoms, respectively, as we clarify below. Furthermore, it is reasonable to assume that the HEI5/6 centers are neither pairing nor clustering defects because we can distinguish only two types or two lattice sites (*k* and *h* sites).

Figure 3 plots the angular dependences of the primary lines of HEI5/6. The HEI5/6 centers have an electron spin of 1/2 and C_{1h} symmetry with respect to the (11$\bar{2}$0) plane. From $S=1/2$, we expect that their charge is either −1 or +1. The charge of −1 is reasonable since HEI5/6 was detected in the *n*-type samples. Table I shows the *g* tensors of HEI5/6 as determined from the fitting of the angular maps (solid lines in Fig. 2).[19] One notable signature is that the main principal value ($g_\parallel$) is larger than the other two; this is a general property of negatively charged centers,[4,6] and it supports the above assignment.

The angular dependences of the HF interactions are the most crucial information for unraveling the microscopic origin of the HEI5/6 centers. Figure 4 shows three angular maps for two rotation planes as well as for two temperatures 295 and 200 K. First, it should be mentioned that the HF inter-

TABLE I. Principal values of g tensor for HEI5/6. θ and ϕ indicate main principal axes (g_{zz} axes) in polar and azimuthal angles. The definition of the Cartesian coordinates is shown in Fig. 5. The g tensors are approximately axial symmetric ($g_{xx} \approx g_{yy}$) and are temperature independent.

Center	Symmetry	g_{xx}	g_{yy}	g_{zz} ($g_{\parallel}$)	θ, ϕ
HEI5	C_{1h}	2.002 42	2.002 58	2.003 45	122°,90°
HEI6	C_{1h}	2.001 85	2.001 75	2.002 39	127°,90°

actions of HEI6 were temperature dependent above 150 K. For example, the HF splitting widths of Si_I were 2.58, 2.80, and 2.90 mT at 295, 200, and 150 K, respectively (for $\mathbf{B} \| [0001]$). Judging from the experimental merits, we analyzed the HEI6 spectra at 295 and 200 K. The 200 K spectra are regarded as a low-temperature limit because the spectral difference between 200 and 150 K was very small (≤ 0.1 mT). The largest HF interaction of HEI5/6 is given by the C_1 atom (see Fig. 4). This HF splitting is maximized for the $[11\bar{2}0]$ direction, indicating that the carbon $2p$ orbital is directed to this direction.

Finally, we performed a fitting of the angular maps by simulating the following spin Hamiltonian:

$$H = \mu_B \mathbf{S} \cdot \mathbf{g} \cdot \mathbf{B} + \mathbf{S} \cdot \mathbf{A} \cdot \mathbf{I} - g_n \beta_n \mathbf{I} \cdot \mathbf{B},$$

where $\mathbf{g}$ is a g tensor and $\mathbf{A}$ is an HF tensor for either the ^{13}C or ^{29}Si nuclear spin.[1] $\mathbf{g}$ was given the values shown in Table I, and only $\mathbf{A}$ was a variable parameter. We assumed axial symmetry for $\mathbf{A}$; i.e., $A_{zz} \equiv A_{\parallel}$ and $A_{xx} = A_{yy} \equiv A_{\perp}$. As shown by the solid lines in Figs. 4(a)–4(c),[19] we successfully fitted the angular patterns of the C_1, Si_I, and Si_{II} HF doublets of HEI6. For example, as shown in Fig. 1(c), the C_1 HF structure splits into four lines with an intensity ratio of 2:4:4:2 for $\mathbf{B} \| [11\bar{2}0]$. This feature has been reproduced in Fig. 4(a). For the $\mathbf{B}$ rotation in the $(11\bar{2}0)$ plane [Figs. 4(b) and 4(c)], the simulation shows that the C_1 HF structure splits into eight blanches with an intensity ratio of 2:2:1:1:1:1:2:2, which is consistent with the observations in Fig. 1(d) and Fig. 2(b), respectively. The determined HF tensors are summarized in Table II. Unfortunately, a full determination was impossible for the Si_I and Si_{II} HF tensors for HEI5 because of a large overlap between the angular patterns of Si_I and Si_{II} [Fig. 4(b)]. We extracted their principal values (corresponding to the minimum and maximum HF splitting widths) and one of their principal coordinates (θ angle), but the other coordinate (ϕ angle) could not be uniquely determined. However, by using the θ and ϕ values predicted by the first-principles calculations (see Table II), we obtained a reasonable agreement between the experiment and simulation for the angular patterns of Si_I and Si_{II}. This ensures that our analyses are reasonable.

Since the assumption of axial symmetry of $\mathbf{A}$ was satisfactory, we can perform a linear combination of atomic orbitals (LCAO) analysis.[1] Namely, the wave function of the unpaired electron of HEI5/6 (Ψ) is expressed by

$$\Psi = \Sigma_i \eta_i [\alpha_i \psi_s + \beta_i \psi_p],$$

where ψ_s and ψ_p are the s and p orbitals of carbon or silicon, α_i and β_i ($\alpha_i^2 + \beta_i^2 = 1$) are the s- and p-orbital fractions of the ith atom, and η_i^2 indicates the total spin density on the ith atom. The LCAO coefficients are calculated as follows:

$$\eta_i^2 \alpha_i^2 = (A_{\parallel} + 2A_{\perp})/3A_0, \quad (1)$$

$$\eta_i^2 \beta_i^2 = (A_{\parallel} - A_{\perp})/3b_0 \quad (2)$$

for each ith atom, where A_0 and b_0 are the HF constants of pure s and p orbitals, respectively.[1] We used $A_0 = 134.77$ mT and $b_0 = 3.832$ mT for ^{13}C and $A_0 = -163.93$ mT and $b_0 = -4.075$ mT for ^{29}Si.[20] The η_i^2 values for the HEI5 and HEI6 (at 200 K) centers were estimated to be, respectively, 54.0% and 52.9% for the C_1 atom, 3.8% and 5.9% for each Si_I atom, and 2.9% and 4.1% for each Si_{II} atom. Namely, the wave function of HEI5/6 is strongly localized on the central C_1 atom, and it weakly extends to four surrounding Si atoms (Si_I and Si_{II}). The sp hybridization ratio on C_1 (β_i^2/α_i^2) is 21.7 (HEI6) or 21.9 (HEI5), which is the largest ratio among the known defects in SiC ($\beta_i^2/\alpha_i^2 = 9.5 \sim 16.4$).[1] The wave function of HEI5/6 on C_1 is very close to a pure $2p$ orbital—in other words, an ideal carbon π orbital. This π orbital should be parallel to the $[11\bar{2}0]$ axis (the $A_{\parallel}$ axis). Such a carbon orbital would never exist in a normal SiC lattice, but it can be generated on an interstitial carbon atom forming sp^2 hybridized bonds in the $(11\bar{2}0)$ plane. Therefore, we conclude that the HEI5/6 centers involve a carbon interstitial atom at the k and h sites in 4H-SiC.

As mentioned above, the first-principles calculation predicted two types of fundamental carbon interstitial defect: dicarbon interstitial $(C_2)_C$ and dicarbon antisite $(C_2)_{Si}$.[9] The former defect is much less stable (much more mobile) than the latter one.[9,10,12] Since the HEI5/6 centers are stable at high temperatures (≤ 1000 °C), as will be demonstrated in Sec. IV, the latter $(C_2)_{Si}$ defects at k or h sites are the most probable origins of HEI5/6. Their charge states should be −1. In Sec. III, this identification is completely confirmed by comparing the HF tensors of the experiment and first-principles calculations. The k and h sites are also distinguished with the help of calculations.

Let us further comment on the temperature dependence of HEI6. Comparing the results for 295 and 200 K, we see that the Si_{II} atom has the largest difference. As in Table II, the main principal axis of $\mathbf{A}(Si_{II})$ exhibits a large variation from $(\theta, \phi) = (119°, 24°)$ to $(117°, 7°)$. This implies that there is a large amount of flexibility or vibration in the vicinity of the Si_{II} atom. Such a characteristic motion seems to bring a faster spin-lattice relaxation on HEI6, resulting in less microwave saturation for HEI6, as mentioned above. In fact, the difference in the microwave saturation behavior between

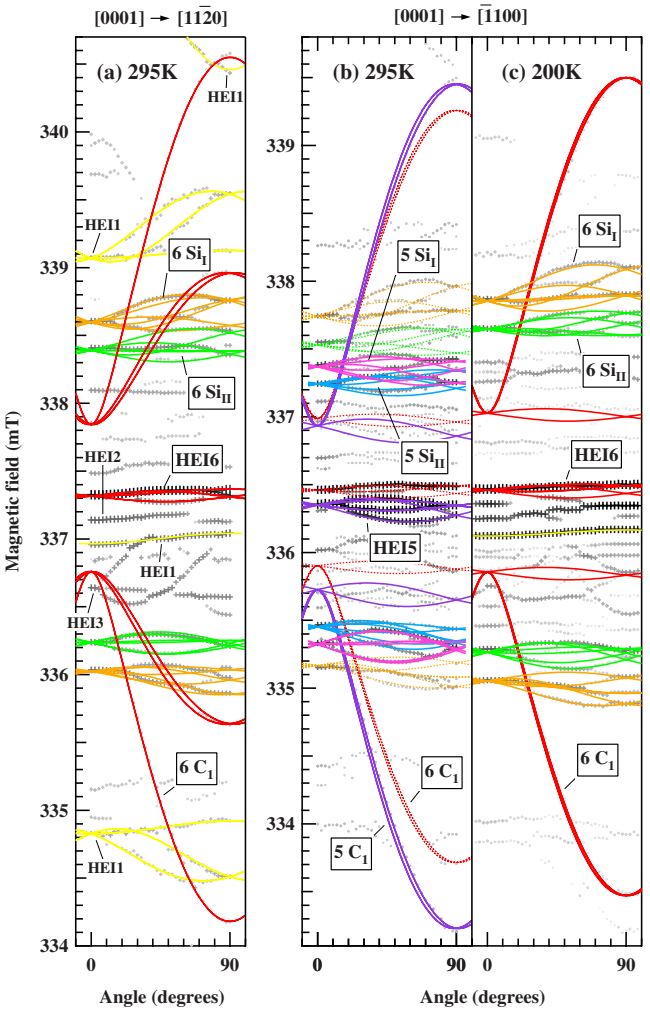

FIG. 4. (Color online) Angular maps for HEI5/6 centers (^{13}C and ^{29}Si hyperfine satellite lines). **B** was rotated either in the ($\bar{1}$100) plane ([0001]→[11$\bar{2}$0]) or in the (11$\bar{2}$0) plane ([0001]→[$\bar{1}$100]). "+" symbols present resonant positions (larger and darker symbols indicate larger resonant peaks). Solid lines were calculated by using the spin-Hamiltonian parameters shown in Tables I and II or by using those in Ref. 4 (for HEI1). "C_1" indicates the ^{13}C hyperfine interaction due to a carbon interstitial atom in HEI5/6. "Si_I" and "Si_{II}" denote ^{29}Si hyperfine interactions from four Si atoms surrounding an interstitial atom (see details in the text). (a) Angular pattern for HEI6 at 295 K. This map was produced using a series of HEI6 spectra shown in Figs. 1(b) and 1(c). (b) Angular patterns for a combination of HEI5 and HEI6 at 295 K. This map was produced using a series of EPR spectra shown in Fig. 2(b). Four inner blanches of C_1 were not resolved due to their small intensities and interferences from many small signals over a middle region [cf. Fig. 2(b)]. Note that the HEI5's pattern was temperature independent, but the HEI6's pattern was temperature dependent above 150 K. (c) Angular pattern of HEI6 at 200 K. This map was produced using a series of HEI6 spectra shown in Fig. 1(d). Four inner blanches of C_1 could not be resolved again. Also some branches of Si_I and Si_{II} were unclear in the map due to overlaps between the satellite lines [cf., Fig. 1(d)]. At this temperature, HEI1/2 signals became larger and disturbed observation of some central lines of HEI6 [cf., Fig. 1(d)].

HEI5 and HEI6 could no longer be observed after lowering the temperature to a point (150 K) at which the HEI6 center became completely frozen.

III. THEORETICAL IDENTIFICATION

We used *ab initio* supercell calculations to study the $(C_2)_{Si}$ defect in detail. Here, we focus mainly on the determination of the HF tensors. For this purpose, we applied the same methodology by which we identified vacancy-related defects in 4*H*-SiC.[4,5] We employed density-functional theory (DFT) within the local-density approximation (LDA) of the Hamiltonian and used the all-electron projector augmented wave method in the calculation of the HF tensors. A detailed explanation and references can be found in our previous publications.[4,5] Here, we briefly describe only the defect modeling that was particularly used for this defect. We applied a 576 atom 4*H*-SiC supercell ($6\times6\times2$ of the primitive unit cell) and the Γ point for *K*-point sampling. This large supercell is certainly sufficient to study an isolated $(C_2)_{Si}$ defect, which has rather delocalized defect states in the gap.[9,10,12] Note that the electrical characteristics were already studied in our previous paper in which we used a method *beyond* that of standard DFT.[12] We found that the $(C_2)_{Si}$ defect is negatively charged in *n*-type SiC and that the positively charged state can be disregarded. Thus, here, we restrict our calculation to the HF tensor of the *negatively charged* $(C_2)_{Si}$ defect. Note that the paramagnetic positively charged state may be detected in moderately doped *p*-type SiC.

The label $(C_2)_{Si}$ indicates a defect in which two carbon atoms share the same Si site (Fig. 5). Hence, such a defect is partially an antisite and an interstitial-related defect. The two carbon atoms in the core (C_1 and C_2 in Fig. 5) bind to two carbon atoms among the four first-neighbor carbon atoms of the Si site. Since the C-C bonds are much shorter than the host Si-C bonds, this defect does not imply stress in the host SiC crystal and only the first- and second-neighbor atoms significantly relax in the lattice. The two carbon atoms in the core have a (graphitic) sp^2-like bonding configuration. Therefore, these carbon atoms have a strongly localized *p* electron pointing perpendicular to the plane defined by the carbon atom in the core and its two first-neighbor carbon atoms. In the neutral state, the two carbon atoms in the core have their own *p* orbital occupied by one electron. Such *p* orbitals are responsible for the defect states appearing in the middle of the gap in 4*H*-SiC. This was already explained in our previous papers[9,12] in which the neutral state was analyzed in detail. We found that the formation energies *and* geometries of the *neutral* $(C_2)_{Si}$ at the *k* and *h* sites of 4*H*-SiC are very similar. In contrast, although the formation energies of the negatively charged $(C_2)_{Si}$ at the *h* and *k* sites are within 0.1 eV, their geometries are not the same [Figs. 5(a) and 5(b)]. In the negatively charged state, the *p* orbital of the C_2 atom (Fig. 5) is filled by two electrons and the system gets frustrated as this *p* orbital repels the *p* orbital of the C_1 atom, and the C_2 atom would like to find an additional partner atom to move from the graphiticlike sp^2 bonding configuration into a sp^3 bonding configuration. This becomes

TABLE II. Spin-Hamiltonian parameters for HEI5/6 centers and negatively charged dicarbon antisites. Measured and calculated principal values of HF tensors are expressed in mT and absolute values. The directions of the main principal axis ($A_{\parallel}$ axis) are indicated with polar and azimuthal angles in Cartesian coordinates. The coordinate system and associated atoms are defined in Fig. 5.

	EPR experiment			First-principles calculation			
Atom	$A_{\perp}$ (A_{xx},A_{yy})	$A_{\parallel}$ (A_{zz})	θ, ϕ	A_{xx}	A_{yy}	A_{zz}	θ, ϕ
		HEI5				$(C_2)^-_{Si}$ at k site	
C_1	1.21	7.15	90°, 0°	1.47	1.50	6.88	90°, 0°
$C_{3,4}$		Not resolved		1.51	1.52	1.91	52°, −64°/−116°
$Si_I \times 2$	1.92	2.24	125°	2.12	2.13	2.54	127°, 23°, 23°/157
$Si_{II} \times 2$	1.78	2.00	88°	1.46	1.47	1.95	82°, 40°/140°
		HEI6 at 200 K (295 K)				$(C_2)^-_{Si}$ at h site	
C_1	1.20	7.02	90°, 0°	1.45	1.47	6.84	90°, 0°
	(1.08)	(6.37)	(90°, 0°)				
$C_{3,4}$		Not resolved		1.89	1.90	2.22	55°,−63°/−117°
$Si_I \times 2$	2.75	3.26	108°, −38°/−142°	3.38	3.39	4.03	109°, −36°/−144°
	(2.53)	(3.00)	(108°, −38°/−142°)				
$Si_{II} \times 2$	2.30	2.63	118°, 24°/156°	2.51	2.53	2.93	118°, 22°/158°
	(2.07)	(2.41)	(117°, 7°/173°)				

possible in the 4*H*-SiC environment by forming a weak "bond" to a second-neighbor Si atom, labeled Si_{back} in Fig. 5. The position of this Si atom at the *h* site is different from its position at the *k* site, and this difference is what leads to the different geometry of this defect. We emphasize that despite the different geometries, the formation energies and one-electron defect levels in the gap of the two sites agree to within 0.1 eV. Now that we have established the geometry of the defect, we are in the position to determine its HF tensor at different sites.

The calculated HF tensors are given in Table II. As usual, the principal values and the azimuthal (θ) and polar (ϕ) angles of the main principal value (A_{zz}) are listed. Note that the strength of the HF constants has a direct relation to the localization of the unpaired electron, as shown in Eqs. (1) and (2). The largest HF constants (hence, the largest localization) are possessed by the C_1 atom (see Fig. 5), which has an unpaired *p* electron, as explained above. We observed measurable HF constants on $C_{3,4}$ atoms and on certain second-neighbor Si atoms, labeled Si_I and Si_{II} in Fig. 5. We measured one large ^{13}C HF signal and two sets of ^{29}Si doublet HF signals.

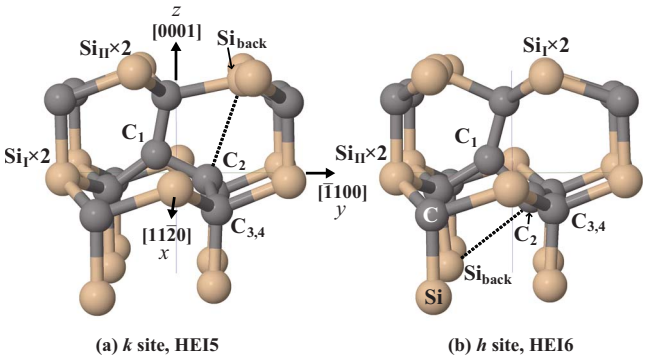

FIG. 5. (Color online) Atomic structures of dicarbon antisites or HEI5/6 centers at *k* and *h* sites in 4*H*-SiC. They have a single negative charge ($S=1/2$) and C_{1h} symmetry with respect to the $(11\bar{2}0)$ plane (*yz* plane). These figures reproduce the atomic positions obtained from the first-principles calculation. The Cartesian coordinate system is also shown in the figure. Note the opposite locations of Si_I and Si_{II} atoms with respect to the C_1 and C_2 atoms between (a) and (b). The dashed line represents the weak interaction between the C_2 atom and a third-neighbor Si atom labeled Si_{back}.

The HF signal from the $C_{3,4}$ atoms would have hardly been observable, judging from the angular-pattern simulation using the theoretical $^{13}C_{3,4}$ HF tensors. For example, the HF splitting widths of $C_{3,4}$ for $\mathbf{B}\|[0001]$ were estimated to be 1.67 mT for HEI5 and 2.01 mT for HEI6, which are close to those of Si_I (2.0 or 2.8 mT) and Si_{II} (1.8 or 2.4 mT) for HEI5/6. The $C_{3,4}$ HF signal would probably be obscured by the Si_I and Si_{II} signals. Because the calculations are valid at 0 K, we compare the low-temperature (200 K) data with the calculated ones in Table II. We found that these sites had very similar HF signals of C_1, and the calculations agree with the experimental data. The Si_I and Si_{II} signals characterize the sites: both the calculations and measurements indicate that HF constants of Si_I and Si_{II} are appreciably lower at the *k* site than at the *h* site. Therefore, we assigned HEI5 to the *k* site and HEI6 to the *h* site. The calculated angles were also close to the measured values, further supporting the idea that the HEI5/6 EPR centers are from negatively charged $(C_2)_{Si}$ defects in 4*H*-SiC. In addition, as shown in Figs. 5(a) and 5(b), the orientations of dicarbon (C_1-C_2) should differ between the sites. The orientation is more tilted from the *c* axis at the *h* site (HEI6). This tilting explains the feature that the $g_{\parallel}$ axis (θ angles in Table I) is more tilted for HEI6 than for HEI5.

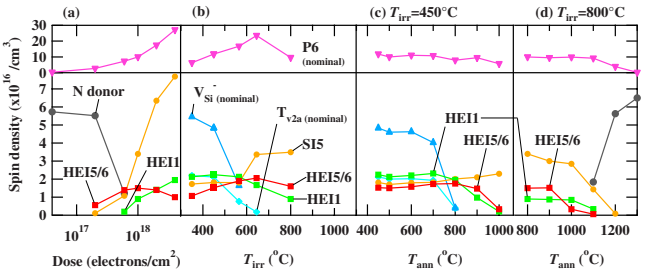

FIG. 6. (Color online) Formation and annihilation of HEI5/6 and other coexisting centers in *n*-type 4*H*-SiC. Panels (a) and (d) are replotted from Ref. 6. (a) Electron dose was varied (zero, 2×10^{17} to 4×10^{18} e/cm^2) for six *n*-type 4*H*-SiC substrates kept at T_{irr}=800 °C. (b) The same dose (1×10^{18} e/cm^2) was applied and the irradiation temperature (T_{irr}) was varied for five *n*-type 4*H*-SiC substrates. (c) and (d) Isochronal annealing measurements for samples of T_{irr}=450 and 800 °C, respectively. Spin densities of N(*k*) donors and HEI5/6 were estimated in the dark at 70 K, while those of SI5 and HEI1 were estimated under photoillumination (100 W halogen light) because these centers were stabilized in EPR-inactive states in the dark. Those of *P*6 and $V_{\mathrm{Si}}^-/T_{V2a}$ are nominal values (respectively, estimated at 30 and 295 K under photoillumination) because they have a triplet (S=1) or a quartet spin (S=3/2) and their EPR signals are enhanced by optically induced spin polarization.

The electronic levels of the $(C_2)_{\mathrm{Si}}$ defects were theoretically investigated in Refs. 9, 11, and 12. In Ref. 12, the electronic structure of $(C_2)_{\mathrm{Si}}$ was calculated *with a correction of the DFT-LDA gap*. The calculated (0/−) and (−/2−) levels in 4*H*-SiC are at $E_C-1.4$ eV and $E_C-0.4$ eV, respectively.[12] In the double negatively charged state, the *p* orbital of the C_1 atom is fully occupied, giving rise a larger repulsion than for the case of $(C_2)_{\mathrm{Si}}^-$. Consequently, the calculated (−/2−) occupation level is about 1.0 eV higher in energy than the (−/0) level. Therefore, the $(C_2)_{\mathrm{Si}}^-$ state is expected to be stable in a wide range of the Fermi-level positions in *n*-type 4*H*-SiC. This explains the observation of HEI5/6 in the thermal equilibrium of our *n*-type samples.

IV. FORMATION AND ANNEALING OF DICARBON ANTISITE

Using the dicarbon antisite model, we examine the formation and annealing of HEI5/6. Figure 6(a) plots the formations of the HEI5/6 centers and other defects as a function of electron dose. Before the irradiation, only a strong N(*k*) donor signal[21] was detectable in the dark, and under photoillumination, a very weak divacancy signal [*P*6, V_CV_{Si} (Ref. 7)] could be recognized below 30 K. In this illuminated state, we did not see the HEI5/6 and other signals. The HEI5/6 centers were immediately formed by the minimum dose of irradiation (2×10^{17} e/cm^2). At this stage, carbon vacancies [HEI1, V_C^- (Ref. 4)] were not yet detectable. The other type of carbon vacancies [SI5, $C_{\mathrm{Si}}V_C^-$ (Ref. 6)] was weakly detected together with the HEI5/6 and N(*k*) signals.[22] This fast formation of HEI5/6 suggests that a number of carbon antisites (C_{Si}) existed before irradiation. In such a situation, mobile carbon interstitials (C_i) could easily produce $(C_2)_{\mathrm{Si}}$ by simply pairing with as-embedded C_{Si} atoms. This idea is in line with the theoretical prediction that C_{Si} is the most abundant defect because of its lowest formation energy, and despite its existence it is optically and electrically invisible due to a lack of electronic levels in the band gap.[9,23] The formation energy of $(C_2)_{\mathrm{Si}}$ was calculated to be 7.8 eV (4*H*-SiC),[10] which is much higher than 4.0–4.2 eV for V_C (Ref. 24) and 3.4 eV for C_{Si}.[9] However, if C_{Si} existed in the *as-grown* samples, the above formation energy for $(C_2)_{\mathrm{Si}}$ should be reduced to 3–4 eV.[9] Existence of C_{Si} in the as-grown samples was also strongly suggested in the PL study where only 3.8 eV photoradiation formed additional $(C_2)_{\mathrm{Si}}$ (the 463 nm PL centers).[14]

Figure 6(b) shows the formations of HEI5/6 and other defects as a function of the irradiation temperature (T_{irr}). The formation of HEI5/6 seems to increase in the range below 650 °C. This is reasonable because at higher temperatures, C_i should diffuse more easily, leading to more $(C_2)_{\mathrm{Si}}$ defects. Furthermore, the formation of HEI5/6 seems to be associated with the annihilation of silicon vacancies [V_{Si}^- and T_{V2a} Ref. 2)] This can be interpreted as V_{Si} defects being transformed into C_{Si} defects as well as into $(C_2)_{\mathrm{Si}}$ defects by capturing C_i atoms.

Figures 6(c) and 6(d) shows isochronal annealing measurements on two different samples (T_{irr}=450 and 800 °C). The HEI5/6 centers of both samples were rapidly annihilated at 1000 °C. This result suggests that at 1000 °C, the $(C_2)_{\mathrm{Si}}$ defects start to dissociate into C_i and C_{Si}, or they themselves start to diffuse. This temperature is much higher than the annihilation temperature of EI1/3 and EI*n* (200–300 °C),[16,17] which probably correspond to dicarbon interstitial defects $(C_2)_C$, and hence the observation is consistent with the theoretical prediction. In Fig. 6(c) (T_{irr} =450 °C), the HEI5/6 and HEI1 (V_C^-) signals were diminished at 1000 °C, which suggests that $(C_2)_{\mathrm{Si}}$ (C_i and C_{Si}) and V_C recombine.

On the other hand, Fig. 6(d) (T_{irr}=800 °C), as well as previous annealing studies,[3,7,25] indicates that the V_C centers were more stable (i.e., stable up to 1100–1500 °C) than $(C_2)_{\mathrm{Si}}$. Accordingly, we expect that the $(C_2)_{\mathrm{Si}}$ defects would be used for building up carbon aggregates rather than for annihilation of V_C. The PL observations strongly support the idea of such an aggregation process occurring. Stable luminescent centers of D_{I}, D_{II}, and many others[15] can be generated by annealing irradiated SiC at higher than 1000 °C. The D_{II} center is believed to originate from one or more C_i and C_{Si} [maybe a family of $(C_2)_{\mathrm{Si}}$],[9,10] and the D_{I} center is expected to involve one or more C_{Si} (probably a sort of antisite clusters).[26–28] The $(C_2)_{\mathrm{Si}}$ defects are closely related to such annealing products. A good example is tricarbon antisite, $(C_3)_{\mathrm{Si}}$,[13,15] which consists of one $(C_2)_{\mathrm{Si}}$ site and one C_i atom. The PL studies showed the tricarbon antisite center (471.8 nm) in irradiated 4*H*-SiC after a 1100–1300 °C anneal[15] and the *U* center (525.0 nm) in irradiated 6*H*-SiC after a 1000–1500 °C anneal.[13] These annealing temperatures are consistent with the activation temperature of $(C_2)_{\mathrm{Si}}$ observed in the present study.

V. SUMMARY

We identified the negatively charged dicarbon antisite defect, $(C_2)_{\mathrm{Si}}^-$, in electron-irradiated *n*-type 4*H*-SiC by means of

combined electron paramagnetic resonance (EPR) measurements and *first-principles* calculations. The HEI5/6 EPR centers ($S=1/2$; C_{1h} symmetry) are associated with cubic and hexagonal dicarbon antisite defects. This assignment is based on a comparison of the measured and calculated hyperfine tensors of ^{13}C and ^{29}Si atoms as far as the second neighborhood around the defect. This defect has a C-C core in $(11\bar{2}0)$ plane and forms a carbon π orbital perpendicular to this plane. An unpaired electron is strongly localized in this orbital, showing a characteristic ^{13}C hyperfine interaction. Although the ^{13}C hyperfine signatures of the cubic and hexagonal sites were the same, the second-neighbor Si atoms and the C-C bond angle were distinguishable between the sites, and this enabled us to identify the two centers. We found that the defects can be created faster than carbon vacancies during electron irradiation. This observation strongly suggests that electrically and optically *inactive* carbon antisite defects existed in the as-grown samples. The formation of $(C_2)_{Si}$ via silicon vacancies was suggested, too. The annealing experiment revealed that the $(C_2)_{Si}$ defects anneal out through recombination of carbon interstitials with vacancies or through formation of carbon aggregates. These processes were activated at about 1000 °C, and this activation temperature is consistent with the formation temperature of various carbon-interstitial-related photoluminescence centers. The calculated occupation levels of $(C_2)_{Si}$ were $E_C-1.4$ eV ($E_V+1.9$ eV) for $(0/-)$ and $E_C-0.4$ eV ($E_V+2.9$ eV) for $(-/2-)$. The calculated $(C_2)_{Si}^-$ state was stable in a wide range of the Fermi-level positions in *n*-type SiC, and this theoretical prediction is consistent with the experimental results.

ACKNOWLEDGMENTS

A.G. acknowledges support from the Hungarian OTKA fund under Contract No. K-67886. We used the Swedish National Super Computer (NSC) (Grant No. snic001-08-22) to carry out the calculations.

[1] J. Isoya, T. Umeda, N. Mizuochi, N. T. Son, E. Janzén, and T. Ohshima, Phys. Status Solidi B **245**, 1298 (2008).
[2] N. Mizuochi, S. Yamasaki, H. Takizawa, N. Morishita, T. Ohshima, H. Itoh, T. Umeda, and J. Isoya, Phys. Rev. B **72**, 235208 (2005).
[3] T. Umeda, J. Isoya, N. Morishita, T. Ohshima, and T. Kamiya, Phys. Rev. B **69**, 121201(R) (2004).
[4] T. Umeda, Y. Ishitsuka, J. Isoya, N. T. Son, E. Janzén, N. Morishita, T. Ohshima, H. Itoh, and A. Gali, Phys. Rev. B **71**, 193202 (2005).
[5] T. Umeda, J. Isoya, T. Ohshima, N. Morishita, H. Itoh, and A. Gali, Phys. Rev. B **75**, 245202 (2007).
[6] T. Umeda, N. T. Son, J. Isoya, E. Janzén, T. Ohshima, N. Morishita, H. Itoh, A. Gali, and M. Bockstedte, Phys. Rev. Lett. **96**, 145501 (2006).
[7] N. T. Son, P. Carlsson, J. ul Hassan, E. Janzén, T. Umeda, J. Isoya, A. Gali, M. Bockstedte, N. Morishita, T. Ohshima, and H. Itoh, Phys. Rev. Lett. **96**, 055501 (2006).
[8] N. T. Son, P. Carlsson, J. ul Hassan, B. Magnusson, and E. Janzén, Phys. Rev. B **75**, 155204 (2007).
[9] A. Gali, P. Deák, P. Ordejón, N. T. Son, E. Janzén, and W. J. Choyke, Phys. Rev. B **68**, 125201 (2003).
[10] A. Mattausch, M. Bockstedte, and O. Pankratov, Phys. Rev. B **69**, 045322 (2004).
[11] M. Bockstedte, A. Mattausch, and O. Pankratov, Phys. Rev. B **69**, 235202 (2004).
[12] A. Gali, N. T. Son, and E. Janzén, Phys. Rev. B **73**, 033204 (2006).
[13] A. Mattausch, M. Bockstedte, O. Pankratov, J. W. Steeds, S. Furkert, J. M. Hayes, W. Sullivan, and N. G. Wright, Phys. Rev. B **73**, 161201(R) (2006).
[14] J. W. Steeds, W. Sullivan, S. A. Furkert, G. A. Evans, and P. J. Wellmann, Phys. Rev. B **77**, 195203 (2008).
[15] J. W. Steeds and W. Sullivan, Phys. Rev. B **77**, 195204 (2008).
[16] N. T. Son, P. N. Hai, and E. Janzén, Mater. Sci. Forum **353-356**, 499 (2001).
[17] M. V. B. Pinheiro, E. Rauls, U. Gerstmann, S. Greulich-Weber, J.-M. Spaeth, and H. Overhof, Mater. Sci. Forum **527-529**, 551 (2006).
[18] T. Umeda, N. Morishita, T. Ohshima, H. Itoh, and J. Isoya, Mater. Sci. Forum **600-603**, 409 (2009).
[19] Simulated files are available in "EPR in Semiconductors:" http://www.kc.tsukuba.ac.jp/div-media/epr/.
[20] J. A. Weil, J. R. Bolton, and J. E. Wertz, *Electron Paramagnetic Resonance* (John Wiley & Sons, NY, 1994).
[21] S. Greulich-Weber, Phys. Status Solidi B **210**, 415 (1998).
[22] The coexistence of the shallow donor signals and the defect signals (HEI5/6, HEI1, and SI5) is a curious behavior because it seems that in some parts the Fermi level stays in shallow donor levels [N(k) level=$E_C-0.092$ eV (Ref. 21)] and in the other parts it is lowered to the defect levels [for example, SI5 level $\sim E_C-1.0$ eV (Ref. 6)]. This kind of behavior was observed in transition processes of the donor compensation [Fig. 6(a), electron dose $<1\times10^{18}/\mathrm{cm}^2$] and the donor recovery [Fig. 6(d), $T_{ann}\leq1200$ °C]. The present observations imply the generation of a nonuniformity in the Fermi level or the defect density inside a specimen during the transition processes. However, confident models are unclear at present and more study will be necessary.
[23] L. Torpo, S. Pöykkö, and R. M. Nieminen, Phys. Rev. B **57**, 6243 (1998).
[24] L. Torpo, T. E. M. Staab, and R. M. Nieminen, Phys. Rev. B **65**, 085202 (2002).
[25] Z. Zolnai, N. T. Son, C. Hallin, and E. Janzén, J. Appl. Phys. **96**, 2406 (2004).
[26] A. Gali, P. Deák, E. Rauls, N. T. Son, I. G. Ivanov, F. H. C. Carlsson, E. Janzén, and W. J. Choyke, Phys. Rev. B **67**, 155203 (2003).
[27] M. V. B. Pinheiro, E. Rauls, U. Gerstmann, S. Greulich-Weber, H. Overhof, and J.-M. Spaeth, Phys. Rev. B **70**, 245204 (2004).
[28] T. A. G. Eberlein, R. Jones, S. Öberg, and P. R. Briddon, Phys. Rev. B **74**, 144106 (2006).